



Cite this: *RSC Adv.*, 2022, 12, 6083

# An efficient modulated synthesis of zirconium metal–organic framework UiO-66†

Xia Chen, Yongjie Li, Qiang Fu, Hongyun Qin, Junnan Lv, Kun Yang, Qicheng Zhang, Hui Zhang and Ming Wang \*

The use of large amounts of deleterious solvents in the synthesis of metal–organic frameworks (MOFs) is one of the important factors limiting their application in industry. Herein, we present a detailed study of the synthesis of UiO-66, which was conducted with hydrobromic (HBr) acid as a modulator for the first time, at a high concentration of precursor solution ( $\text{ZrCl}_4$  and  $\text{H}_2\text{BDC}$ , both  $0.2 \text{ mol L}^{-1}$ ). Powder crystals with atypical cuboctahedron structure were obtained which indicated that the HBr acid modulator played roles by competitive coordination and deprotonation modulation, thereby controlling the processes of nucleation and crystal growth. The properties of the obtained materials were systematically characterized and compared with those of materials synthesized with hydrofluoric (HF) acid and hydrochloric (HCl) acid modulators. Despite the high concentration of defectivity, the UiO-66 material synthesized with the HBr acid additive has the characteristics of larger specific surface area, excellent thermal stability and higher porosity in the structure. Besides that, the present protocol has the advantages of high reaction mass efficiency (RME), and feasibility of scalable synthesis, providing a facile and sustainable route to diverse Zr-based MOFs.

Received 24th October 2021  
Accepted 10th February 2022

DOI: 10.1039/d1ra07848h

rsc.li/rsc-advances

## 1. Introduction

Metal–organic frameworks (MOFs), which have garnered increasing attention due to their numerous applications in fields such as gas storage/separation, luminescent sensing, drug delivery and photocatalysis, constitute a class of microporous materials with high specific area, flexible structure and tunable properties.<sup>1–7</sup> Zirconium-based MOFs represented by UiO-66 (UiO for University of Oslo) are a fascinating family of robust porous materials with excellent stability. Owing to the high oxytropic nature of  $\text{Zr(IV)}$  (coordinated by 8 oxygen atoms or ions) and the very close-packed coordination of secondary building units (SBUs, coordinated with 12 linker molecules), UiO-66 is claimed to have excellent thermal stability and chemical stability which makes it highly resistant to solvents such as water, DMF, benzene and acetone.<sup>8–10</sup> All these advantages are precisely the disadvantages of many other MOFs, making these compounds unattractive for many industrial applications.

The synthesis of UiO-66 have been carried out successfully in DMF by solvothermal method.<sup>8,11</sup> However, reducing or even omitting costly organic solvents but maintaining high yield is the prerequisites for large-scale industrial applications.<sup>12</sup>

Hence, it is necessary to study the synthesis process and the corresponding properties of UiO-66 in high concentration of precursors solution. Besides that, the properties of porous crystal materials are closely related to its morphology, and the precise control of which is still challenging. Crystal morphology can be deliberately modulated through chemical reaction route as well as crystal nucleation and growth rates during synthesis.<sup>13,14</sup> Modulation approach, which was originally invented by the group of Kitagawa,<sup>15,16</sup> has been shown to improve the reproducibility of the synthesis of Zr-based MOFs, enhance the crystallinity of the products and in some cases allow control over the particle size.<sup>15,17</sup> Certain Zr-based MOFs can in fact only be obtained using modulation.<sup>18–20</sup> Modulating agent, usually an inorganic or organic acid, regulates the deprotonation rate of organic linkers or competes with the linkers for coordination sites at the metal centers which are described as deprotonation mechanism and coordination mechanism, respectively. The modulator reduces crystal nucleation and growth rates, yielding a better control over the MOFs formation. Hydrochloric (HCl) acid is the most studied inorganic acid modulator.<sup>21–23</sup> With the presence of hydrofluoric (HF) acid, Guo and co-workers<sup>17</sup> have successfully synthesized UiO-66 with morphologies of cuboctahedron, which underwent a competitive coordination with organic linkers. Indeed, the acidity of haloid acid modulators and the base hardness of its anions affect the deprotonation rate of ligands and the bonding strength between the anions and Zr ions, which ultimately change the overall rate of crystallization.<sup>17,18,24</sup> The

School of Chemistry and Chemical Engineering, Shandong University of Technology, Zibo 255000, China. E-mail: wangmingmw@sdut.edu.cn

† Electronic supplementary information (ESI) available. See DOI: 10.1039/d1ra07848h



corresponding structure and performance of MOFs will also change. In fact, previous studies were carried out in low concentrations of precursors solution that were generally not higher than  $0.05 \text{ mol L}^{-1}$ .<sup>8,17,25–27</sup> The effects of high concentration of reactants on the yield and morphology of the prepared materials were seldom reported.<sup>28</sup> To the best of our knowledge, the effects of hydrobromic (HBr) acid modulator in the synthesis of UiO-66 and the applicable of the modulating mechanism of modulators at high concentration have not been reported. According to the hard and soft acid/base theory (HSAB), the bond formed between Zr and Br ions is the weakest among F, Cl and Br ions. Br ions bonded to Zr in the SBUs, which compensate for the charge imbalance of frameworks, are the easiest to be replaced by BDC. The exchange of linkers which can ultimately reduce the linker-missing defects caused by other haloid acid or the saturated precursors solution. Moreover, highly acidic HBr could compete with the organic linkers to coordinate with the Zr metal centers, thereby controlling the processes of nucleation and growth of the UiO-66 crystals.

Herein, the modulating effects of HBr acid on the yield, morphology and other properties of UiO-66 crystals synthesized from high concentration of reagents were systematically studied. A comparative approach, taking into account the aforementioned properties of the resulting materials, was employed to study the modulating effects of inorganic haloid acid modulators including HF, HCl and HBr acid. The resulting materials were carefully characterized and the modulation mechanism as well as the changes in structure and properties of UiO-66 crystals caused by the introduction of halogen atoms was also studied. In addition, a larger-scale synthesis was conducted and the “greenness” of the process was also assessed. The study will help for furthering the practical application of MOFs in such fields as adsorption and so on.

## 2. Experimental sections

### 2.1 General information

Zirconium tetrachloride ( $\text{ZrCl}_4$ , 99.95 wt%), 1,4-benzenedicarboxylic acid ( $\text{H}_2\text{BDC}$ , 99 wt%) and  $N,N$ -dimethylformamide (DMF, 99.9 wt%) were provided by J&K scientific Co. Ltd. Hydrobromic acid (HBr, 40 wt%), hydrochloric acid (HCl, 37 wt%), hydrofluoric acid (HF, 40 wt%) and anhydrous methanol (MeOH, 99.5 wt%) were purchased from Shanghai Aladdin Biochemical technology Co. Ltd. All chemicals were used without further purification.

### 2.2 Characterization of UiO-66

X-ray diffraction (XRD) data were collected at room temperature by using a conventional high-resolution ( $\theta$ - $2\theta$ ) diffractometer (D8-ADVANCED, Bruker) with Cu-K $\alpha$  radiation at a scanning rate of  $0.2^\circ \text{ s}^{-1}$  from  $3^\circ$  to  $50^\circ$ . The size and morphology of UiO-66 crystals were imaged by a field-emission scanning electron microscopy (Quanta 250 FEG, FEI). FT-IR spectra of the samples were recorded by a Nicolet 5700 spectrometer (thermoelectric) in the range of  $50$ – $7800 \text{ cm}^{-1}$ . The elemental composition and

the corresponding chemical states of UiO-66 was characterized by X-ray Photoelectron Spectroscopy (XPS, Thermo Fisher ESCALAB XI+). Thermogravimetric analysis (TGA) was performed in the flux of air using DTG-60 thermogravimetric analyzer (Shimadzu) in the range of  $25$ – $800^\circ \text{C}$  at  $10^\circ \text{C min}^{-1}$ . Surface area and pore characteristics were determined by ASAP 2460 analyzer (Micromeritics) using  $\text{N}_2$  at  $77 \text{ K}$ . Prior to the measurements, all the samples were degassed at  $150^\circ \text{C}$  for  $10 \text{ h}$ .

### 2.3 Solvothermal synthesis of UiO-66

The synthesis of UiO-66 was based on the previous report<sup>11</sup> with some changes in the concentration of precursors solution ( $0.2 \text{ mol L}^{-1}$ , limit of the solubility of precursors in DMF<sup>29</sup>). Equimolar  $\text{ZrCl}_4$  ( $0.930 \text{ g}$ ,  $4 \text{ mmol}$ ) and organic ligand  $\text{H}_2\text{BDC}$  ( $0.660 \text{ g}$ ,  $4 \text{ mmol}$ ) were separately dissolved in total  $20 \text{ mL}$  DMF under ultrasound for  $30 \text{ minutes}$ . The two solutions were then mixed by ultrasonic stirring for  $10 \text{ minutes}$ . To study the influence of modulators including HF acid, HCl acid and HBr acid,  $1$ – $9$  molar equivalents of inorganic acid to  $\text{ZrCl}_4$  (denoted as “eq.”, Table S1†) was then added with additional  $5 \text{ minutes}$  ultrasound. The obtained solution was loaded into a  $50 \text{ mL}$  Teflon-lined steel autoclave and then heated at  $120^\circ \text{C}$  for  $24 \text{ h}$ . The produced white powders were harvested by  $5000 \text{ rpm}$  centrifugation for certain time, thoroughly washed with anhydrous methanol three times to remove the extra reactants and DMF encased in the pore, then dried at  $150^\circ \text{C}$  for  $10 \text{ h}$  to remove the solvents. The samples were labelled as UiO-66-free for sample synthesized without modulator and UiO-66- $n\text{HF}$ , UiO-66- $n\text{HCl}$ , UiO-66- $n\text{HBr}$  for samples synthesized with acidic additive where  $n$  was the molar ratio of haloid acid to  $\text{ZrCl}_4$  ( $n = 1$ – $9$ ). The reaction mass efficiency (RME, %, eqn (1)) was employed to evaluate the process efficiency.<sup>25,30</sup>

$$\text{RME} = \frac{m_{\text{UiO-66}}}{m_{\text{Zr}} + m_{\text{linker}}} \times 100 \quad (1)$$

where  $m_{\text{UiO-66}}$ ,  $m_{\text{Zr}}$  and  $m_{\text{linker}}$  are masses of materials prepared and starting materials ( $\text{ZrCl}_4$  and  $\text{H}_2\text{BDC}$  linkers), respectively.

## 3. Results and discussion

### 3.1 Structure and properties of haloid acid-promoting synthesized UiO-66

SEM images of selected samples synthesized with HBr acid additive were presented in Fig. 1. The resulting crystals did not exhibit well-defined morphology, but existed in form of heterogeneous agglomerates with atypical cuboctahedron structure. It may be mainly due to the relatively low pressure under the saturation condition.<sup>17,31</sup> Increasing amount of HBr acid modulator resulted in the acceleration of crystallization rate. As shown in Fig. 1, however, no significant differences were observed in particle size and degree of agglomeration. It indicates that the modulating effects of HBr acid on decreasing the growth rate of crystals were not obvious, although it did increase the nucleation rate significantly. Based on the four processes of UiO-66 fabrication described by Xu and coworkers,<sup>32</sup> the assemble of multinuclear clusters from the formed hexanuclear SBU with organic ligand  $\text{H}_2\text{BDC}$  in UiO-66



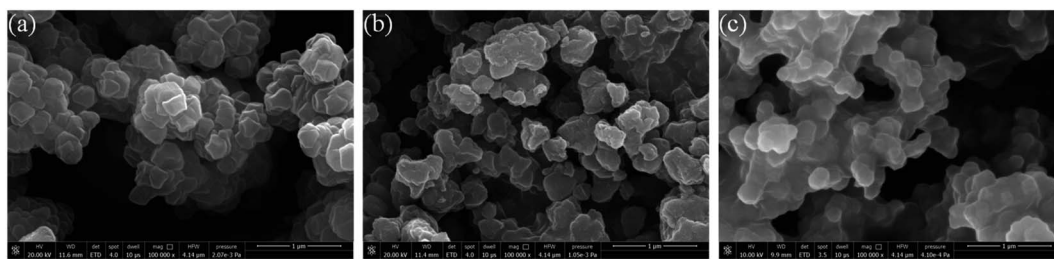


Fig. 1 SEM images of samples synthesized with (a) 1 eq. of HBr acid; (b) 5 eq. of HBr acid; (c) 9 eq. of HBr acid.

homogeneous precursor solution took place in a relatively short period of time, whereas the assembly was impeded by the high concentration precursors. It may be one of the reasons for the formation of linker-missing defects. After heating applied, the aggregation of multi-clusters which has been observed to be existed as an independent process before fully crystallization took place quickly and underwent growth gradually.

XRD patterns of the as-synthesized samples modulated by HBr acid were shown in Fig. 2a. As can be seen, all samples exhibited characteristic diffraction peaks of UiO-66 at  $7.4^\circ$ ,  $8.5^\circ$  and  $25.8^\circ$ ,<sup>8,17</sup> which were significantly different from sample UiO-66-free (Fig. 2b). Moreover, the samples presented narrower and sharper diffraction peaks by introducing HBr acid in the reaction system. However, with the increase of HBr acid dosage, differences were not immediately obvious for all samples including the  $2\theta$  region around the (111) (the strongest and ideally the first) reflection of UiO-66 (*ca.*  $7.4^\circ$   $2\theta$ ). The crystallite size derived from the (111) reflection (FWHM the reflection) according to Schaler's formula<sup>33</sup> was almost constant and was independent of the molar ratio HBr/Zr (Fig. 3 and Table S3†), basically in agreement with the SEM observation (Fig. 1). This may be ascribed to the accelerated nucleation of Zr oxoclusters by 40 wt% HBr acid, thus changing the crystallization process from nucleation-limited to growth-limited crystallization.<sup>15,33,34</sup> In addition, UiO-66-2HF and UiO-66-2HCl samples showed similar particle size as UiO-66-HBr samples, indicating the same controlling step (Fig. 3 and Table S3†).

At the low-angle range of  $2\theta$  *ca.*  $2\text{--}7^\circ$ , a broad-peak was additionally observed in the XRD profiles of all samples which was assigned to the (110) reo phase or cluster-missing

defects.<sup>24,33</sup> Strong acidic modulators (HCl acid,  $pK_a = -8.00$ ; HBr acid,  $pK_a = -9.00$ ;  $H_2BDC$ ,  $pK_{a1} = 3.51$ ,  $pK_{a2} = 4.82$ ) dominate the competition for carboxylate sites on the  $Zr_6O_4(OH)_4(CO_2)_{12}$  clusters, resulting in samples with a very high concentration of cluster-missing defects.<sup>24</sup>  $Rel(I)_{B.P.}$  usually used to represent the relative intensity of the broad peak was exclusively associated with the defectivity of cluster-missing and was calculated as eqn (2).<sup>24,35</sup> The results were presented in Fig. 3 and Table S2.†

$$Rel(I)_{B.P.} = \frac{I_{B.P.}}{\frac{I(111) + I(200) + I(600)}{3}} \times 100 \quad (2)$$

where  $I_{B.P.}$ ,  $I(111)$ ,  $I(200)$  and  $I(600)$  are the intensity of diffraction peaks at  $2\text{--}7^\circ$ ,  $7.4^\circ$ ,  $8.5^\circ$  and  $25.8^\circ$ , respectively.

As shown in Fig. 3, the defectivity of cluster-missing exhibited an almost completely opposite trend to the crystallite size with the exception UiO-66-5HBr. Under the high concentration precursors condition, the cluster-missing defects likely originated from the kinetic regulation rather than the equilibrium in ligands competitive coordination. Of course, the formation of this type of defects was also highly correlated with the crucial role of water.<sup>33</sup> At a limited accessibility to water molecules, the metastable species  $[Zr_4(OH)_8(H_2O)_{16}]^{8+}$  may be formed upon rapid hydrolysis of  $ZrCl_4$  that allow a lower coordination with ligands and play a role of pre-nucleation species for the formation of the reo domain.<sup>33</sup> The particularity of sample UiO-66-5HBr may be due to the fact that chloride ion has been completely replaced by bromide ions to coordinate with  $Zr_6$  or  $Zr_4$  clusters, and charges of the system were balanced.

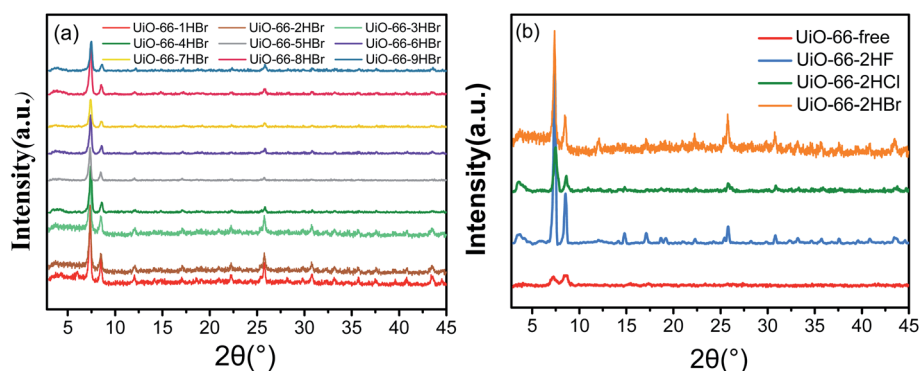


Fig. 2 XRD patterns of UiO-66 modulated synthesis by (a) HBr acid; (b) certain amount of different haloid acid.



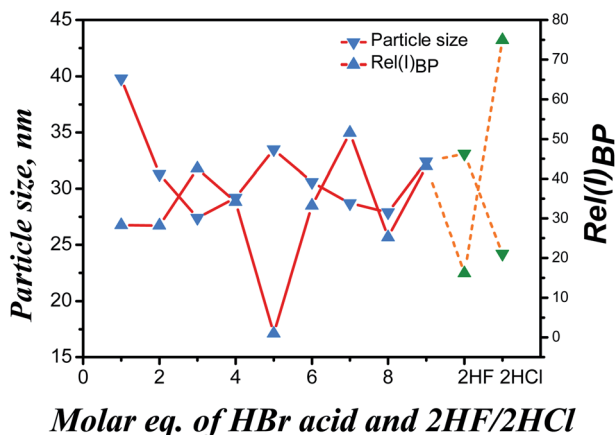


Fig. 3 Particle size and relative intensity of (110) reo peak for samples UiO-66-*n*HBr (solid line), UiO-66-2HF and UiO-66-2HCl (dash line).

Comparison of XRD patterns of samples synthesized with different type of acidic modulators is shown in Fig. 2b. As can be seen, the three selected samples all exhibited intense characteristic diffraction peaks of UiO-66 at  $7.4^\circ$ ,  $8.5^\circ$  and  $25.8^\circ$ . Materials obtained with HF acid and HBr acid modulators, especially the fluorine-involved sample, exhibited better crystallinity than those with HCl additive. Compared with other haloid ions, fluoride ion with strong affinity for  $\text{Zr}^{4+}$  competed with  $\text{H}_2\text{BDC}$  ligand and coordinated with  $\text{Zr}_6$  cluster which, to some extent, slowed down rate of nucleation and crystal growth, reduced amount of nucleation and improved crystallinity of materials.<sup>17</sup> Comparison of the three typical samples (Fig. 3) indicated that the fluorine-involved sample (dash lines) had the lowest cluster-missing defectivity, while the chlorine-involved sample showed the opposite which was higher than any bromine-involved sample (solid lines). The particularity of fluorine-involved sample may be attributed to the similar acidity of HF acid ( $\text{p}K_{\text{a}} = 3.18$ ) with  $\text{H}_2\text{BDC}$  ( $\text{p}K_{\text{a}1} = 3.51$ ) but stronger acidity than HBDC ( $\text{p}K_{\text{a}2} = 4.82$ ). Fairly close competition between HF acid and the singly deprotonated linker ( $\text{HBDC}^-$ ) allows HF acid to behave more like a modulator in the traditional sense, inhibit crystal nucleation and promoting its growth.<sup>15,24,36,37</sup> On the other hand, the moderate amount of cluster-missing defects may be generated because more deprotonated modulator molecules (HF acid), which still “win” many of the carboxylate sites on the  $\text{Zr}_6(\text{OH})_4\text{O}_4(\text{CO}_2)_{12}$  clusters, were existed than doubly deprotonated linker molecules ( $\text{BDC}_2^-$ ).<sup>24</sup>

The FT-IR spectra of UiO-66-free, UiO-66-2HF, UiO-66-2HCl, UiO-66-2HBr and  $\text{H}_2\text{BDC}$  are compared in Fig. 4. The peaks of the as-prepared UiO-66 occurred in positions similar to reported values.<sup>38,39</sup> Peaks at  $1586$ ,  $1396\text{ cm}^{-1}$  and  $1506$ ,  $746\text{ cm}^{-1}$  are characteristic vibration of  $\text{C}=\text{O}$  bond and aromatic ring, respectively. The broad peak at  $3103\text{--}2546\text{ cm}^{-1}$  are due to the vibration of carboxyl group.<sup>39,40</sup> The sample UiO-66-free exhibited very weak vibration peaks at  $1506\text{ cm}^{-1}$  (vibration of  $\text{C}=\text{C}$  in aromatic ring) and  $480\text{ cm}^{-1}$  (vibration of  $\text{Zr-O}_{\text{u}3}\text{-OH}$  bond in the  $\text{Zr}_6$  cluster) indicating high defectivity and poor crystallinity of the material.<sup>17</sup> For samples prepared with haloid acid

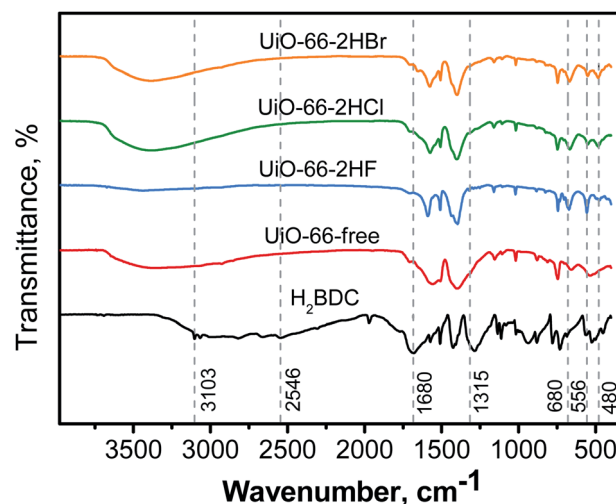


Fig. 4 FT-IR spectra of the organic linker  $\text{H}_2\text{BDC}$ , samples UiO-66-free, UiO-66-2HF, UiO-66-2HCl and UiO-66-2HBr.

modulator, however, there was no evident vibration peak at  $3103\text{--}2546\text{ cm}^{-1}$ . In addition, it was actually not observed the pendant coordinated-free carboxylate group (vibration peak at around  $1680\text{ cm}^{-1}$  assigned to  $\nu\text{C}=\text{O}$  and  $1315\text{ cm}^{-1}$  assigned to  $\nu\text{C-OH}$ ), suggesting carboxyl groups of  $\text{H}_2\text{BDC}$  molecule could react almost completely in the presence of modulator.<sup>31,41</sup> The vibration peak of  $\text{Zr-O}$  at around  $680\text{ cm}^{-1}$  as well as at about  $480\text{ cm}^{-1}$  were other evidences for the formation  $\text{Zr}_6$  clusters and for the coordination occurred between  $\text{Zr}^{4+}$  and carboxyl groups of  $\text{H}_2\text{BDC}$ .<sup>9,17</sup> Hence, it can be considered that BDC molecule has been chemically bonded to the framework of UiO-66 and the presence of certain haloid ions did not affect the composition of functional groups in UiO-66.

To further explore the effects of haloid ions on Zr-MOFs, the elements and the corresponding chemical states have been studied from XPS spectra. We here take UiO-66-2HBr as an example. The XPS spectrum of UiO-66-2HBr shows that it is composed of Zr, C, and O (Fig. 5a). The spectra of Zr 3d of UiO-66 can be deconvoluted to two peaks of Zr  $3d_{3/2}$  and Zr  $3d_{5/2}$  at  $182.95$  and  $185.40\text{ eV}$  (Fig. 5b). The characteristic peaks at  $283.56$  and  $530.46\text{ eV}$  are attributed to C 1s and O 1s orbitals of UiO-66-2HBr, respectively.<sup>42</sup> The above results show that zirconium and oxygen elements exist in the form of  $\text{Zr(IV)}$  and  $\text{O}^{2-}$ , respectively. In addition, the XPS spectra also indicated the presence of  $\sim 1.90\%$  residual chlorine and  $\sim 0.29\%$  bromine that played the role in charge balance in the framework.

TGA curves of all samples synthesized with HBr acid additive are presented in Fig. 6a by rescaling the weight at the end of the process to 100% and attribute it to pure  $\text{ZrO}_2$  phase. As can be seen, all samples exhibited a nearly continuous weight loss up to around  $350^\circ\text{C}$ , and the TGA plateaus were observed in the  $350\text{--}450^\circ\text{C}$  interval, which followed by the complete decomposition of frameworks at around  $550^\circ\text{C}$ . The first significant weight loss below  $100^\circ\text{C}$  associated with solvent and water desorption, while the second and third weight-loss periods could be attributed to Zr cluster dehydration and linker loss, respectively.<sup>17,40</sup> Fig. 6b presented the TGA comparison of



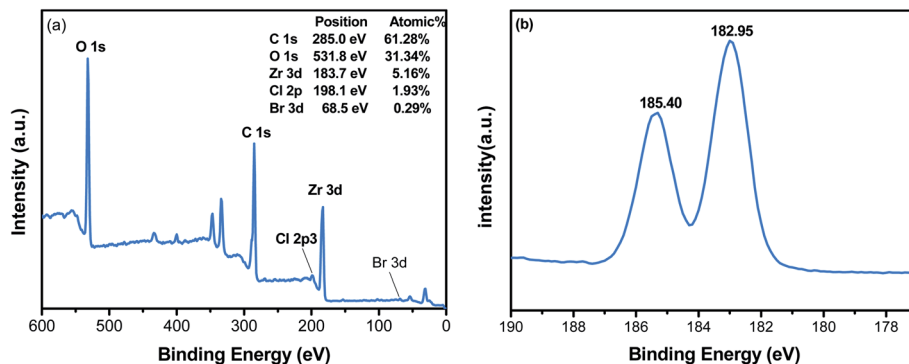


Fig. 5 XPS spectra of UiO-66-2HBr: (a) survey spectrum; (b) Zr 3d.

typical samples modulated with different haloid acid. Similar weight-loss was observed except for the first step. Samples synthesized with HBr and HCl acid additive showed greater weight loss than those with HF acid. It may be explained by the fact that fluorine with stronger electronegativity has priority to occupy the oxygen defect position caused by linker deficiency, and thus making F ions relatively difficult to be replaced by water or DMF or organic linker molecule as the crystal grows.<sup>17</sup> The strong bond strength of Zr–F also implies a higher framework decomposition temperature of fluorine-involved samples than fluorine-free samples which were clearly observed in Fig. 8b. On the other hand, Zr–Br and Zr–Cl bonds are less stable than Zr–F and Zr–O bonds, especially Zr–Br bond. This was confirmed by TGA results that samples synthesized with HCl and HBr additive showed no significant change on the decomposition temperature compared to the sample without acid additive.

The thermal stability of UiO-66 was negatively and severely affected due to the existence of deficiency including cluster-missing defects and linker-missing defects.<sup>24,26,43</sup> The concentration of cluster-missing defects has been confirmed by the results of XRD patterns. TG method was usually performed to quantitatively analyze the organic content, further the number of missing linkers could be calculated according to the magnitude of the decomposition weight loss step.<sup>9,17,26,44</sup> As shown in

Fig. 6a, the magnitude of the decomposition weight loss was significantly lower than that of theoretically expected in all samples (weight difference between  $\text{Zr}_6\text{O}_6(\text{BDC})_6$  light grey dot line and the pure  $\text{ZrO}_2$  line, 131.4%), indicating they were linkers deficient. It is worth noting that TG method is known to be less accurate for the quantitative analysis of the organic content.<sup>45</sup> However, as shown in Fig. 6a and Table S4,<sup>†</sup> for all samples except UiO-66-1HBr, the larger the amount of modulator was used, the more pronounced the linkers deficiency tended to be. The linker-missing deficiency of the as-synthesized bromine-involved samples ranged from about 18.51% (4.9BDC, experimental coordination number) to 27.25% (4.4BDC) (Table S4<sup>†</sup>). For chlorine-involved sample UiO-66-2HCl, it exhibited similar TG curve but higher missing linker defects concentration (4.6BDC, 23.46%) compared with sample UiO-66-2HBr (4.9BDC, 18.51%). Corresponding to the higher thermal decomposition temperature, fluorine-involved sample UiO-66-2HF showed a lower linker-missing defects concentration (5.3BDC, 11.67%) which may contribute to its excellent thermal stability.

### 3.2 Morphology-dependent porosity of UiO-66

To explore the influence of powder crystal morphology on the pore structure of UiO-66 at different modulating condition,

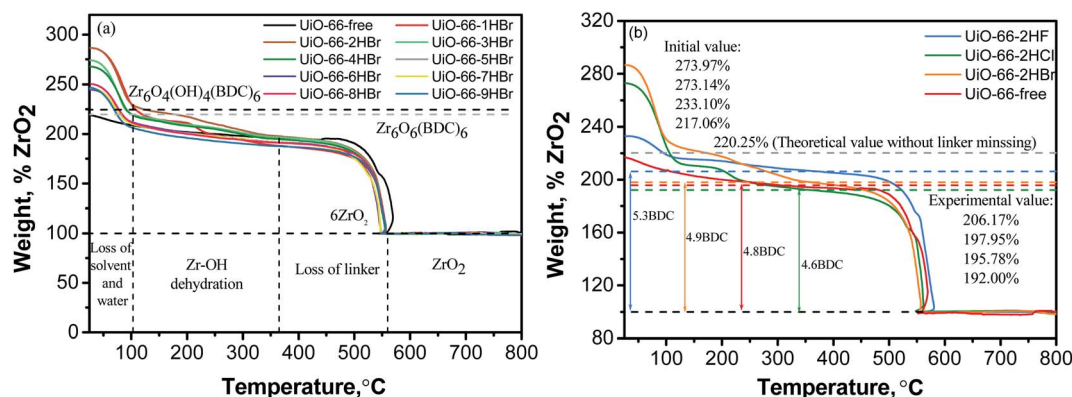


Fig. 6 TGA curves of UiO-66 synthesized (a) with HBr acid modulator; (b) without and with HF, HCl acid modulators. The normalized weight of the hydrated and dehydrated samples was represented by gray and black dotted lines, respectively.

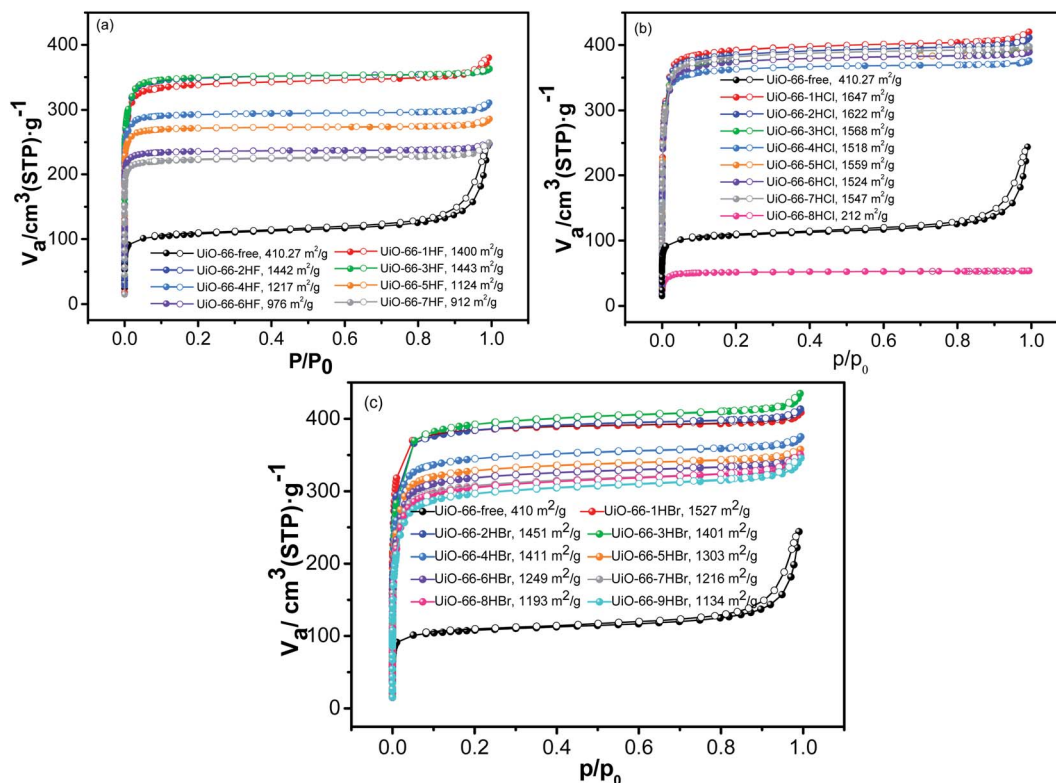


Fig. 7 Nitrogen adsorption isotherms obtained on UiO-66 samples modulated synthesis by (a) HF acid; (b) HCl acid; and (c) HBr acid at 77 K. Adsorption and desorption are represented by filled and open icons, respectively.

nitrogen ( $N_2$ ) adsorption was performed at 77 K on the activated UiO-66 samples. The  $N_2$  adsorption/desorption isotherms of almost all UiO-66 samples (Fig. 7) could be attributed to type-I (IUPAC classification). The steep increase in the low-pressure range and plateau in the high-pressure range suggest an overall microporous nature for these samples. As shown in Fig. 7,

the  $N_2$  uptake was greatly depended on the type and the amount of modulator used. With the absence of modulator, the sample UiO-66-free (black curve in all three plots) was considerably less porous than all those synthesized with modulator. Of even greater interest was the observation of two remarkable conspicuous trends: (1) With the increase of modulator dosage,

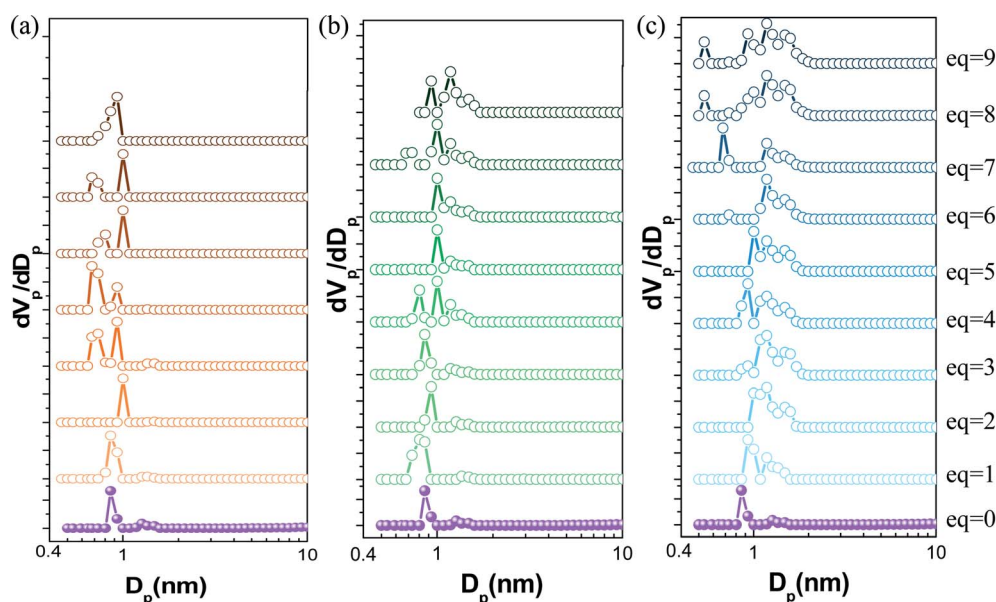


Fig. 8 Pore size distribution (PSD) profiles derived by NLDFT of all samples modulated by (a) HF acid; (b) HCl acid; and (c) HBr acid.



the adsorption capacity (thus porosity) of samples presented certain regularity related with the type and amount of modulator. (2) The uptake and porosity of samples was sensitive to modulator amount with the descending order of HF, HBr and HCl acid. As HBr acid dosage got higher, the porosity of UiO-66 samples showed a trend of first very slightly increasing (1–3 eq.) and then decreasing much more (4–9 eq.). However, the increasing dosage of HF acid resulted in the significant decrease of UiO-66 porosity which was quite different from samples obtained with HCl acid additive. More specially, when the amount of HCl was too large (8–9 eq.), the adsorption performance declined sharply, or even did not occur. It can be attributed to the facts that excessive amount of modulator resulted in samples with high concentration of defectivity which would undoubtedly lead to the instability of samples.<sup>40</sup>

Similarly, BET surface area presented a significant increasement from 410 m<sup>2</sup> g<sup>−1</sup> of the modulator-free sample to 1647 m<sup>2</sup> g<sup>−1</sup> of UiO-66-1HCl sample. More importantly, the trend in porosity (now quantitatively described by BET surface area, Fig. 7 and Table S5†) influenced by modulator type and dosage were almost the same as that described by adsorption uptake. Under the same conditions, BET of the samples synthesized with HF acid modulator was relatively minimum, while those synthesized with HCl acid was relatively maximum. Take samples UiO-66-2HF, UiO-66-2HCl and UiO-66-2HBr for example, BET surface area values were 1442, 1622 and 1451 m<sup>2</sup> g<sup>−1</sup>, respectively. The larger the haloid acid-ZrCl<sub>4</sub> ratio was, the greater difference in BET surface areas was. For samples UiO-66-*n*HBr (*n* = 1–9), BET surface areas were afforded values of 1527, 1451, 1401, 1411, 1303, 1249, 1216, 1193 and 1134 m<sup>2</sup> g<sup>−1</sup> with the increase of *n*, respectively. The decrease of BET may be attributed to their instability caused by poor crystalline structure.<sup>40</sup>

The pore size distributions (PSD) were constructed by NLDFT method for all samples and were presented in Fig. 8. As can be seen, the PSD of UiO-66-free were relatively centralized at 9.3 Å which was slightly larger than that typically reported for defect-free UiO-66 (theoretical calculated value 9 Å).<sup>46,47</sup> With the increase amount of acid additive, the heterogeneity of samples' PSD increased to varying degrees, especially those modulated by HBr acid. When UiO-66 was synthesized with 1–5 eq. HBr acid additive, the pore size distribution exhibited a slight broad peak with a small shoulder. The peak was positioned at around 10.0 Å. Such an enlarged pore size has been reported for UiO-66 with linker-missing defects where the shortage of the linkers from the metal cluster expanded the entire framework.<sup>46–48</sup> With the increase amount of HBr acid, a variety of modes of pore larger than 10 Å were equipped and the largest of which was up to 15.9 Å. The appearance of the 15.9 Å pores was associated with the removal of clusters in an octahedral cavity formation.<sup>40,46,48–50</sup> When HBr-ZrCl<sub>4</sub> molar ratio was larger than 6, the heterogeneity of pores further increased. A new mode of pores positioned at around 6 Å appeared which theoretically the triangular window connecting the regular octahedral cavity (about 11 Å) and the regular tetrahedral cavity (about 8 Å).<sup>8,51</sup> High concentration of cluster-missing defects increased the formation of octahedral cavity with smaller coordination number and lower

steric hindrance, resulting in the simultaneous appearance of heterogenetic pores between ~6 Å and ~15.9 Å. These results agreed well with the observation of reo topology by XRD (Fig. 2) and of atypical cuboctahedron structure by SEM (Fig. 1). Based on all the above observations, it may be concluded that both of linker-missing and cluster-missing defects co-existed in the HBr-promoted samples. For the fluorine-involved samples, pores at around 6 Å corresponding to cluster-missing defectivity appeared besides those at around 9 Å when the molar ratio of HF to ZrCl<sub>4</sub> was not less than 3. In contrast, the pore size of chlorine-involved samples additionally exhibited another mode of larger pore (no larger than 12 Å). The difference between PSD of the as-synthesized samples induced by acid type may be attributed to the difference in the strength and bonding number of halogen-Zr bonds caused by basic hardness of haloid ions.

### 3.3 Influence of haloid acid modulators on the reaction mass efficiency (RME) of UiO-66

Modulators play important roles in the synthesis of MOFs, such as influencing crystal morphology, RME and so on.<sup>26,33,40,52</sup> The effect of haloid acid on RMEs of UiO-66 synthesized with 0.2 mol L<sup>−1</sup> ZrCl<sub>4</sub> was also investigated and the results were presented in Fig. 9 (Table S1†). As can be seen, trace amount of UiO-66 (RME 18.21%) was formed in the absence of modulator only, which was not unexpected as water in modulator was a requisite for the formation of the Zr<sup>4+</sup> oxo/peroxo clusters (SBU, Zr<sub>6</sub>O<sub>4</sub>(OH)<sub>4</sub>).<sup>34</sup> The ZrCl<sub>4</sub>-H<sub>2</sub>O molar ratio of 6 : 8 (eqn (3)) is theoretically required for the formation of Zr<sub>6</sub>O<sub>4</sub>(OH)<sub>4</sub>(BDC)<sub>6</sub>.<sup>25</sup> 1 eq. of HBr acid provided an adequate amount of water (ZrCl<sub>4</sub>-H<sub>2</sub>O molar ratio was about 6 : 10) required to form the SBUs of UiO-66. However, the dosage of HF acid and HCl acid was 4 eq. and 2 eq., respectively.

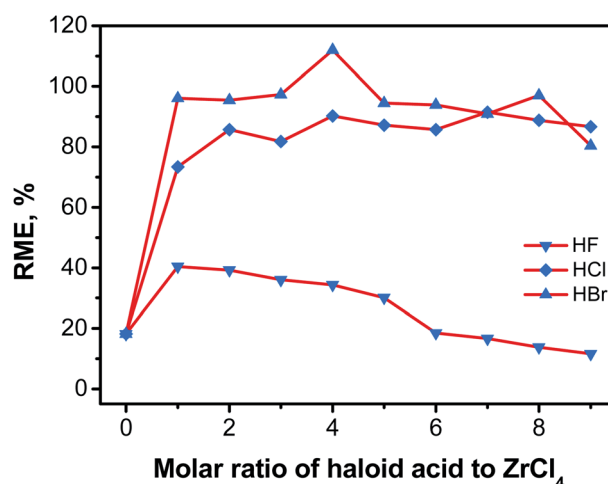
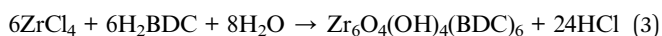


Fig. 9 The RMEs of UiO-66 synthesized with different haloid acid modulator.

Table 1 The scale-up synthesis of UiO-66-2HBr

Sample designation	Molar equivalents/masses (g) or volume (mL)				Mass of products/g	RME, %
	ZrCl <sub>4</sub> /g	H <sub>2</sub> BDC/g	DMF/mL	HBr acid/mL		
UiO-66-2 HBr	1/0.9325	1/0.6602	64.6/20.0	2/0.430	1.52	95.44
UiO-66-2 HBr <sub>su</sub>	3/2.7992	3/1.9824	193.8/60.0	6/1.290	3.95	84.52
	3/2.7930	3/1.9885	193.8/60.0	6/1.290	4.02	
	3/2.7905	3/1.9867	193.8/60.0	6/1.290	4.15	

Consequently, the nucleation rate and crystallization rate increased significantly with the addition of the modulator. A large amount of white powder products appeared within 30 minutes even if only 1 eq. of HBr acid was used. By comparison, it took 5–6 hours for any crystal to emerge without additives. It was obvious that the introduction of HBr acid was beneficial to crystal nucleation and growth. Moreover, the RMEs of UiO-66 synthesis exhibited a small change (94.50–97.31%) as the dosage of HBr acid modulator increased from 1 eq. to 9 eq., except for UiO-66-4HBr. Similar conclusions appeared for HCl acid as modulator. However, HCl acid was proved to be slightly inferior to HBr acid in accelerating the crystallization. The RMEs of UiO-66-*n*HCl samples were concentrated at 85–90% lower than those of UiO-66-*n*HBr samples with same amount of acidic additive. Interestingly, HF acid showed completely different influence on the RMEs of UiO-66-*n*HF. As the mole ratio of HF-ZrCl<sub>4</sub> increases, the RMEs decreased monotonically with the maximum value of only 40.39%. In addition, when the amount of modulators was too large (eq.  $\geq 7$ ), the RMEs of UiO-66 synthesized with HCl and HBr acid additive decreased slightly to different degree. In fact, materials obtained with HF acid additive was only about 15 percent of those obtained with HCl or HBr acid additive. Stronger acidity caused by the relatively small amount of water inhibited the formation of SBU, thus reducing the concentration of Zr<sub>6</sub> multinuclear species together with the products yield.<sup>32</sup> The different influence of the three acidic modulators on the overall crystallization rate and RME may be attributed to the difference in the amount of water,

acidity of modulator and vapor pressure caused by solvent.<sup>24,32</sup> Other factors, such as strength of chemical bond formed between Zr<sup>4+</sup> and halide ions which affect the rate and extent of the coordination between Zr<sup>4+</sup> and organic linker BDC, may also play key roles in the acid modulating process.<sup>17</sup>

In order to assess the industrial applicability and greenness of this process, the results of scale-up synthesis (take UiO-66-2HBr as example and labelled as UiO-66-2HBr<sub>su</sub>) were presented in Table 1, and the accessible green chemistry metrics such as RME, and environmental factor (*E* factor) for the synthesis of UiO-66-2HBr<sub>su</sub> were quantified. For the larger-scale synthesis, scale was increased by a factor of 3. Reaction conditions for scale-up synthesis followed the same trend as the small-scale synthesis. As shown in Table 1, the results of larger scale experiments proved that the average RME was 84.52%. We further made a comparison with the traditional synthesis reported previously<sup>44</sup> (Fig. 10). As seen in Fig. 10, the synthesis of UiO-66-2HBr<sub>su</sub> gave the best *E* factor and RME metrics compared to previous work. It is noteworthy that the synthesis gave a low value of *E* factor (30.3 kg kg<sup>-1</sup>), while the traditional low precursor concentration synthesis gave higher values of *E* factor (108.3 kg kg<sup>-1</sup>). Such a remarkable difference is mainly due to the reduction in solvent usage in UiO-66 synthesis. By comparing these results, it can be seen that the present process shows great advantage in greenness compared with the traditional protocols.

## 4. Conclusions

Discussion of overall findings, the foremost conclusions of the study are as follows:

(1) Zirconium-based MOFs UiO-66 with significant amounts of missing Zr<sub>6</sub> clusters was synthesized with HBr acid modulator at high concentration of precursors solution (0.2 mol L<sup>-1</sup>). Despite the high concentration of defectivity, the as-synthesized UiO-66 samples had the characteristics of high RME, larger specific surface area, excellent thermal stability and higher porosity compared with materials synthesized by HCl acid and HF acid modulators.

(2) UiO-66-*n*HBr samples were existed in the form of heterogeneous agglomerates with atypical cuboctahedron structure which was similar to the chlorine- or fluorine-involved samples. The crystallite size was almost constant and not depending on the ratio HBr/Zr. The results indicated that haloid acid modulators' effects of competitive coordination or deprotonation modulation on decreasing the rate of nucleation and

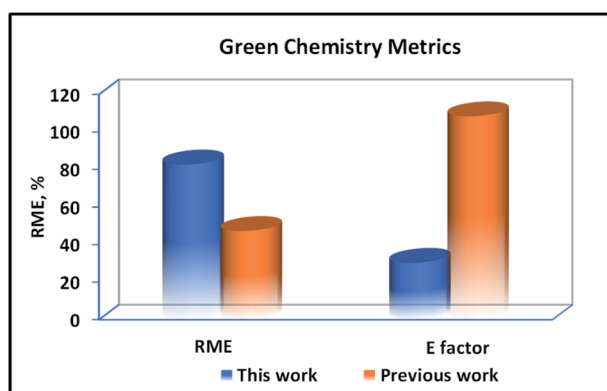


Fig. 10 Comparative graphical plot of green chemistry metrics calculated for the synthesis of UiO-66.



growth of crystal were not obvious under the high concentration condition. With the increase of the amount of haloid acid additive, however, the samples' defectivity and porosity (quantitatively described by N<sub>2</sub> adsorption uptake and BET surface areas) increased in varying amplitude.

(3) We successfully scaled up the synthesis of UiO-66-2HBr by a factor of 3, resulting in an average RME of 84.52%. Considering such metrics as RME and *E* factor, the present process also shows great advantage in greenness compared with the traditional protocols. It could be considered as a step forward in the request for large-scale synthesis and industrial application of Zr-MOFs.

## Conflicts of interest

The authors declare no competing financial interest.

## Acknowledgements

The authors greatly appreciate the financial support of Natural Science Foundation of Shandong province (Grant No. ZR2020MB121).

## References

- 1 H. C. Zhou and S. Kitagawa, *Chem. Soc. Rev.*, 2014, **43**, 5415–5418.
- 2 H. Kim, S. Yang, S. R. Rao, S. Narayanan, E. A. Kapustin, H. Furukawa, A. S. Umans, O. M. Yaghi and E. N. Wang, *Science*, 2017, **356**, 430–434.
- 3 H. Furukawa, K. E. Cordova, M. O'Keeffe and O. M. Yaghi, *Science*, 2013, **341**, 1230444.
- 4 A. Cadiau, Y. Belmabhout, K. Adil, P. M. Bhatt, R. S. Pillai, A. Shkurenko, C. Martineau-Corcus, G. Maurin and M. Eddaoudi, *Science*, 2017, **356**, 731–735.
- 5 H. Furukawa and O. M. Yaghi, *J. Am. Chem. Soc.*, 2009, **131**, 8875–8883.
- 6 A. Corma, H. García and F. X. Llabrés i Xamena, *Chem. Rev.*, 2010, **110**, 4606–4655.
- 7 V. V. Butova, V. A. Polyakov, A. P. Budnyk, A. M. Aboraia, E. A. Bulanova, A. A. Guda, E. A. Reshetnikova, Y. S. Podkovyrina, C. Lamberti and A. V. Soldatov, *Polyhedron*, 2018, **154**, 457–464.
- 8 J. H. Cavka, S. Jakobsen, U. Olsbye, N. Guillou, C. Lamberti, S. Bordiga and K. P. Lillerud, *J. Am. Chem. Soc.*, 2008, **130**, 13850–13851.
- 9 L. Valenzano, B. Civalieri, S. Chavan, S. Bordiga, M. H. Nilsen, S. Jakobsen, K. P. Lillerud and C. Lamberti, *Chem. Mater.*, 2011, **23**, 1700–1718.
- 10 Z. J. Chen, S. L. Hanna, L. R. Redfern, D. Alezi, T. Islamoglu and O. K. Farha, *Coord. Chem. Rev.*, 2019, **386**, 32–49.
- 11 Z. G. Hu, Y. W. Peng, Z. X. Kang, Y. H. Qian and D. Zhao, *Inorg. Chem.*, 2015, **54**, 4862–4868.
- 12 G. Zahn, H. A. Schulze, J. Lippke, S. König, U. Sazama, M. Fröba and P. A. Behrens, *Microporous Mesoporous Mater.*, 2015, **203**, 186–194.
- 13 M. W. Terban, D. Banerjee, S. Ghose, B. Medasani, A. Shukla, B. A. Legg, Y. F. Zhou, Z. H. Zhu, M. L. Sushko, J. J. De Yoreo, J. Liu, P. K. Thallapally and S. J. L. Billinge, *Nanoscale*, 2018, **10**, 4291–4300.
- 14 A. E. Platero-Prats, A. Mavrandonakis, L. C. Gallington, Y. Y. Liu, J. T. Hupp, O. K. Farha, C. J. Cramer and K. W. Chapman, *J. Am. Chem. Soc.*, 2016, **138**, 4178–4185.
- 15 A. Schaate, P. Roy, A. Godt, J. Lippke, F. Waltz, M. Wiebcke and P. Behrens, *Chem.–Eur. J.*, 2011, **17**, 6643–6651.
- 16 T. Tsuruoka, S. Furukawa, Y. Takashima, K. Yoshida, S. Isoda and S. Kitagawa, *Angew. Chem., Int. Ed. Engl.*, 2009, **48**, 4739–4743.
- 17 Y. T. Han, M. Liu, K. Y. Li, Y. Zuo, Y. X. Wei, S. T. Xu, G. L. Zhang, C. S. Song, Z. C. Zhang and X. W. Guo, *CrystEngComm*, 2015, **17**, 6434–6440.
- 18 G. Wißmann, A. Schaate, S. Lilienthal, I. Bremer, A. M. Schneider and P. Behrens, *Microporous Mesoporous Mater.*, 2012, **152**, 64–70.
- 19 A. Schaate, P. Roy, T. Preusse, S. J. Lohmeier, A. Godt and P. Behrens, *Chem.–Eur. J.*, 2011, **17**, 9320–9325.
- 20 A. Schaate, S. Dühnen, G. Platz, S. Lilienthal, A. M. Schneider and P. Behrens, *Eur. J. Inorg. Chem.*, 2012, **5**, 790–796.
- 21 Z. J. Chen, X. J. Wang, H. Noh, G. Ayoub, G. W. Peterson, C. T. Buru, T. Islamoglu and O. K. Farha, *CrystEngComm*, 2019, **21**, 2409–2415.
- 22 M. J. Katz, Z. J. Brown, Y. J. Colón, P. W. Siu, K. A. Scheidt, R. Q. Snurr, J. T. Hupp and O. K. Farha, *Chem. Commun.*, 2013, **49**, 9449–9451.
- 23 J. H. Qiu, Y. Feng, X. F. Zhang, M. M. Jia and J. F. Yao, *J. Colloid Interface Sci.*, 2017, **499**, 151–158.
- 24 G. C. Shearer, S. Chavan, S. Bordiga, S. Svelle, U. Olsbye and K. P. Lillerud, *Chem. Mater.*, 2016, **28**, 3749–3761.
- 25 R. Vakili, S. J. Xu, N. Al-Janabi, P. Gorgojo, S. M. Holmes and X. L. Fan, *Microporous Mesoporous Mater.*, 2018, **260**, 45–53.
- 26 V. V. Butova, O. A. Burachevskaya, I. V. Ozhgin, G. S. Borodkin, A. G. Starikov, S. Bordiga, A. Damin, K. P. Lillerud and A. V. Soldatov, *Microporous Mesoporous Mater.*, 2020, **305**, 110324–110332.
- 27 L. A. Lozano, C. M. Iglesias, B. M. C. Faroldi, M. A. Ulla and J. M. Zamaro, *J. Mater. Sci.*, 2018, **53**, 1862–1873.
- 28 Z. S. Moghaddam, M. Kaykhani, M. Khajeh and A. R. Oveisi, *Spectrochim. Acta, Part A*, 2018, **194**, 76–82.
- 29 D. Q. Li, D. Z. Liu and F. A. Wang, *J. Chem. Eng. Chin. Univ.*, 2001, **15**, 258–261.
- 30 M. Taddei, P. V. Dau, S. M. Cohen, M. Ranocchiari, J. A. van Bokhoven, F. Costantino, S. Sabatini and R. Vivani, *Dalton Trans.*, 2015, **44**, 14019–14026.
- 31 J. Xu, J. Liu, Z. Li, X. B. Wang, Y. F. Xu, S. S. Chen and Z. Wang, *New J. Chem.*, 2019, **43**, 4092–4099.
- 32 H. Xu, S. Sommer, N. L. N. Broge, J. K. Gao and B. B. Iversen, *Chem.–Eur. J.*, 2019, **25**, 2051–2058.
- 33 P. Chammingkwan, G. Y. Shangcum, L. T. T. Mai, P. Mohan, A. Thakur, T. Wada and T. Taniike, *RSC Adv.*, 2020, **10**, 28180–28185.
- 34 F. Ragon, P. Horcajada, H. Chevreau, Y. K. Hwang, U. H. Lee, S. R. Miller, T. Devic, J. S. Chang and C. Serre, *Inorg. Chem.*, 2014, **53**, 2491–2500.

- 35 M. J. Cliffe, J. A. Hill, C. A. Murray, F. X. Coudert and A. L. Goodwin, *Phys. Chem. Chem. Phys.*, 2015, **17**, 11586–11592.
- 36 D. W. Feng, K. C. Wang, Z. W. Wei, Y. P. Chen, C. M. Simon, R. K. Arvapally, R. L. Martin, M. Bosch, T. F. Liu, S. Fordham, D. Q. Yuan, M. A. Omary, M. Haranczyk, B. Smit and H. C. Zhou, *Nat. Commun.*, 2014, **5**, 5723.
- 37 M. Bosch, M. W. Zhang and H. C. Zhou, *Adv. Chem.*, 2014, **2014**, 1–8.
- 38 H. Hu, H. X. Zhang, Y. Chen, Y. J. Chen, L. Zhuang and H. S. Ou, *Chem. Eng. J.*, 2019, **368**, 273–284.
- 39 D. Y. Yu, M. H. Wu, Q. Hu, L. L. Wang, C. C. Lv and L. Zhang, *J. Hazard. Mater.*, 2019, **367**, 456–464.
- 40 L. J. Wang, X. H. Wen, J. Li, P. Zeng, Y. H. Song and H. Z. Yu, *Chem. Eng. J.*, 2021, **405**, 126681–126692.
- 41 M. B. Hay and S. C. B. Myneni, *Geochim. Cosmochim. Acta*, 2007, **71**, 3518–3532.
- 42 Y. H. Cao, X. G. Chen, X. Li and B. Wang, *ACS Appl. Nano Mater.*, 2021, **4**, 5486–5495.
- 43 J. Canivet, M. Vandichel and D. Farrusseng, *Dalton Trans.*, 2016, **45**, 4090–4099.
- 44 G. C. Shearer, S. Forselv, S. Chavan, S. Bordiga, K. Mathisen, M. Bjørgen, S. Svelle and K. P. Lillerud, *Top. Catal.*, 2013, **56**, 770–782.
- 45 Y. Y. Liu, R. C. Klet, J. T. Hupp and O. Farha, *Chem. Commun.*, 2016, **52**, 7806–7809.
- 46 F. Vermoortele, B. Bueken, G. Le Bars, B. Van de Voorde, M. Vandichel, K. Houthoofd, A. Vimont, M. Daturi, M. Waroquier, V. Van Speybroeck, C. Kirschhock and D. E. De Vos, *J. Am. Chem. Soc.*, 2013, **135**, 11465–11468.
- 47 B. Shan, S. M. McIntyre, M. R. Armstrong, Y. X. Shen and B. Mu, *Ind. Eng. Chem. Res.*, 2018, **57**, 14233–14241.
- 48 H. Wu, Y. S. Chua, V. Krungleviciute, M. Tyagi, P. Chen, T. Yildirim and W. Zhou, *J. Am. Chem. Soc.*, 2013, **135**, 10525–10532.
- 49 M. Vandichel, J. Hajek, F. Vermoortele, M. Waroquier, D. E. De Vos and V. Van Speybroeck, *CrystEngComm*, 2015, **17**, 395–406.
- 50 M. J. Cliffe, W. Wan, X. D. Zou, P. A. Chater, A. K. Kleppe, M. G. Tucker, H. Wilhelm, N. P. Funnell, F. X. Coudert and A. L. Goodwin, *Nat. Commun.*, 2014, **5**, 4176–4183.
- 51 S. Chavan, J. G. Vitillo, D. Gianolio, O. Zavorotynska, B. Civalieri, S. Jakobsen, M. H. Nilsen, L. Valenzano, C. Lamberti, K. P. Lillerud and S. Bordiga, *Phys. Chem. Chem. Phys.*, 2012, **14**, 1614–1626.
- 52 G. R. Cai and H. L. Jiang, *Angew. Chem., Int. Ed. Engl.*, 2017, **56**, 563–567.

